Published in final edited form as:
*Biochemistry*. 2011 August 16; 50(32): 7033–7044. doi:10.1021/bi200456u.

# A Transient Kinetic Analysis of PRMT1 Catalysis

**You Feng**[≠], **Nan Xie**[≠], **Miyeong Jin**[≠], **Mary R. Stahley**[#], **James T. Stivers**[#], and **Yujun George Zheng**[≠,*]

[≠]Department of Chemistry, Georgia State University, PO Box 4098, Atlanta, Georgia 30302

[#]Department of Pharmacology and Molecular Sciences, Johns Hopkins University, 725 N. Wolfe Street, Baltimore, MD 21205

## Abstract

Posttranslational modifications (PTMs) are important strategies used by eukaryotic organisms to modulate their phenotypes. One of the well studied PTMs, arginine methylation, is catalyzed by protein arginine methyltransferases (PRMTs) with SAM as the methyl donor. The functions of PRMTs have been broadly studied in different biological processes and diseased states, but the molecular basis for arginine methylation is not well defined. In this study, we report the transient-state kinetic analysis of PRMT1 catalysis. The fast association and dissociation rates suggest that PRMT1 catalysis of histone H4 methylation follows a rapid equilibrium sequential kinetic mechanism. The data give direct evidence that the chemistry of methyl transfer is the major rate-limiting step, and that binding of the cofactor SAM or SAH affects the association and dissociation of H4 with PRMT1. Importantly, from the stopped-flow fluorescence measurements, we have identified a critical kinetic step suggesting a precatalytic conformational transition induced by substrate binding. These results provide new insights into the mechanism of arginine methylation and the rational design of PRMT inhibitors.

### Keywords

PRMT1; arginine methylation; transient-state kinetics; conformational transition; fluorescent probe; stopped flow

Arginine methylation of the core histones is catalyzed by protein arginine methyltransferases (PRMTs), which transfer the methyl group from S-adenosyl-L-methionine (SAM) to the guanidino group of specific arginine residues. Thus far, about nine PRMT members have been identified at the proteomic level in mammalian cells and these have been grouped into two major types (type I and type II) according to their product specificity (1–3). Type I enzymes (PRMT1, 2, 3, 4, 6, and 8) catalyze the transfer of the methyl group from SAM to one guanidino nitrogen atom of arginine residue to produce ω-$N^G$ monomethylarginines (MMA, L-NMMA) and ω-$N^G$,$N^G$-asymmetric dimethylarginines (ADMA) [for a review, see a ref. (4)]. Type II enzymes (*e.g.*, PRMT5) catalyze the formation of MMA and ω-$N^G$, $N'^G$-symmetric dimethylarginines (SDMA) (5–8). As a result of the methyl transfer, SAM is converted to the product S-adenosyl-L-homocysteine (SAH). PRMTs can exhibit quite high substrate specificity which is correlated with their different specific functions. For instance,

*To whom correspondence should be addressed: PO BOX 4098, Atlanta, GA 30302-4098. Telephone: (404)413-5491. Fax: (404) 413-5505. yzheng@gsu.edu.

SUPPORTING INFORMATION AVAILABLE

Additional data about the fluorescence titration of H4FLme1-PRMT1 complex with H4(1–20), the $k_{obs}$ versus PRMT1 concentration plots for H4FL and H4FLme2, and the time course of H4FLme2 dissociation from PRMT1-SAM complex. This material is available free of charge via the Internet at http://pubs.acs.org.

CARM1 (PRMT4) methylates H3R2, H3R17 and H3R26 (9, 10), while PRMT1 and PRMT5 specifically methylate H4R3 and H3R8 (11, 12). The methylation at distinct sites can affect the status of gene expression differently. For instance, asymmetric dimethylation at H3R17 and H4R3 stimulates gene activation, whereas symmetric dimethylation at H4R3 is associated with gene repression (11, 13, 14). In general, PRMT-catalyzed arginine methylation is essential for many biological processes including gene transcriptional regulation (9, 11–13, 15–17), signal transduction (18–21), RNA transport (8, 22), RNA splicing (23, 24), DNA repair, and embryonic development and cellular differentiation (25–27).

Several studies of the kinetic mechanism of arginine methylation have been recently reported. One steady-state kinetic analysis suggested that PRMT1 utilizes a rapid equilibrium random mechanism (RER) for methyl transfer with the formation of dead-end EAP and EBQ complexes (28). In another study, PRMT6 was shown to follow an ordered sequential mechanism in which SAM binds to the enzyme first and the methylated product is the first to dissociate (29). The slight difference in these two studies may suggest that kinetics of arginine methylation can vary slightly among the individual isoforms. Nevertheless, both studies support a sequential kinetic mechanism in which a ternary complex is formed prior to the methyl transfer step.

Many important questions about the PRMT-catalyzed arginine methylation reaction remain to be answered. For instance, it is not known whether the chemical step or a protein conformational change in the ES complex is rate-limiting for catalysis. Such a molecular level understanding of how substrate recognition is coupled to catalysis will be of great significance to evaluate the function of PRMT activity in different physiological contexts. To address these mechanistic questions, transient kinetic analyses of arginine methylation are highly desirable. Unfortunately, such studies are greatly limited by lack of assay tools appropriate for fast measurement of substrate binding and methylation on rapid time-scales. In particular, routine radioisotope-labeled methyl transfer assays do not provide information about conformational events along the reaction coordinate. Recently, we reported fluorescently labeled peptide substrates that could be useful in studies of substrate binding and methylation (30). Here we report that such substrates serve as excellent tools to dissect the transient kinetic events during PRMT1 catalysis. By using fluorophore-labeled H4 substrates in combination with stopped flow measurements, we have determined the microscopic rate constants for the key binding and methylation steps during PRMT1 catalysis. This study provides kinetic evidence that substrate recognition induces a conformational transition of the active site of PRMT1, and strongly indicates that the methyl transfer step is overall rate-limiting for arginine methylation. In addition, we find that binding of the cofactor SAM/SAH modulates the interaction between PRMT1 and the peptide substrate.

## EXPERIMENTAL PROCEDURES

### Design and synthesis of modified H4 peptides

The amino-terminal peptide of histone H4 containing the first 20 amino acid residues, with different methylation patterns and a fluorescein group were synthesized using Fmoc [N-(9-fluorenyl) methoxycarbonyl]-based solid phase peptide synthesis (SPPS) protocol on a PS3 peptide synthesizer (Protein Technology. Tucson, AZ) as described previously (31). Each amino acid was coupled to the solid phase with 4 equivalents of amino acid/HCTU [O-(1H-6-Chlorobenzotriazole-1-yl)-1,1,3,3-tetramethyluronium hexafluorophosphate] (Novabiochem, Darmstadt, Germany). The Fmoc group was deprotected with 20% v/v piperidine/DMF, and the N-terminal amino acid was acetylated with acetic anhydride. The peptide was cleaved from the Wang resin by a cleavage solution consisting of 95%

trifluoroacetic acid (TFA), 2.5% $H_2O$ and 2.5% triisopropylsilane. It was then precipitated in cold ether and pelleted by centrifuge. Crude peptides were collected and purified using a Varian Prostar instrument equipped with a C18 Reversed-phase High Performance Liquid Chromatography (RP-HPLC) column, where 0.05% TFA-containing water and 0.05% TFA-containing acetonitrile were two mobile phases used in gradient purification. The purity and identity of peptides were confirmed by MALDI-MS. For the peptides linked to a fluorescein group, their concentrations were calibrated according to the absorption of fluorescein at 492 nm.

### Expression and purification of PRMT1

Recombinant His-tagged rat PRMT1 was expressed in *E. coli* and purified with Ni-charged His6x-tag binding resin as reported previously (32). Briefly, the PRMT1-pET28b plasmid was transformed into *BL21(DE3)* (Stratagene). Transformed bacteria were incubated in LB media at 37°C for growth, and then 16°C for protein expression which was induced by 0.3 mM IPTG. Cells were harvested by centrifuge and lysed by French Press. The supernatant containing PRMT1 protein was loaded onto the Ni-charged His6x-tag binding resin (Novagen) that was equilibrated with column buffer (25 mM Na-HEPES, pH 7.0, 300 mM NaCl, 1 mM PMSF, and 30 mM imidazole). Beads were washed thoroughly with column buffer, followed by washing buffer (25 mM Na- HEPES, pH 7.0, 300 mM NaCl, 1 mM PMSF, and 70 mM imidazole), and protein was eluted with elution buffer (25 mM Na-HEPES, pH 7.0, 300 mM NaCl, 1 mM PMSF, 100 mM EDTA, and 200 mM imidazole). Different eluent fractions were checked by 12% SDS-PAGE, and PRMT1 concentration was determined by Bradford assay.

### Chemical crosslinking and Western blotting of PRMT1 oligomers

To study the relationship between PRMT1 oligomerization and concentration, His6x-rPRMT1 was diluted in the range of 0.012 μM ~ 3.13 μM with storage buffer (25 mM HEPES (pH 7.0), 250 mM NaCl, 1 mM EDTA, 10% glycerol, and 1 mM DTT) containing 0.1% Triton X-100, and incubated at 4 °C overnight. Then PRMT1 was cross-linked with 0.025% (v/v) glutaraldehyde at room temperature for 5 min. The reactions were quenched by addition of SDS loading buffer, and PRMT1 proteins were separated by 8% SDS-PAGE followed by western blot detection, with anti-PRMT1 rabbit polyclonal IgG (Upstate) as the primary antibody and goat anti-rabbit IgG-HRP (Millipore) as the secondary antibody. After washing away the unbound probes, PRMT1 bands were visualized using the SuperSignal West Pico Trial Kit (Thermo Scientific). The film image was analyzed by *Quantity One*, and the molar fraction of PRMT1 monomer, dimer and oligomer were plotted against PRMT1 concentration.

### Radioactive methyltransferase assay

The methylation assays of different H4 peptides or protein were performed using $^{14}C$-isotope labeled SAM at 30°C. The reaction buffer contained 50 mM HEPES (pH 8.0), 50 mM NaCl, 1mM EDTA and 0.5 mM DTT. H4 substrate and [$^{14}C$]-SAM were preincubated in the reaction buffer for 5 min prior to initiation of the methyl transfer reaction by adding PRMT1 (0.01 μM typically). The reaction time was controlled under initial rate conditions such that typical reaction yields were less than 20%. The reaction was quenched by spotting the reaction mixture on P81 filter paper disc (Whatman). After the paper discs were washed with 50 mM $NaHCO_3$ (pH 9.0) and air dried, liquid scintillation counting was performed to measure the amount of methylated products. Values for $K_m$ and $k_{cat}$ were obtained by measuring the initial velocity of the reaction at various concentrations of one substrate and fixed saturating concentration of the other substrate (cofactor). The kinetic data were fitted to the Michaelis-Menton equation using non-linear regression methods.

### Equilibrium fluorescent titration

The $K_d$ value for PRMT1 and the fluorescent peptide binding was measured by fluorescence anisotropy methods. Increasing concentrations of PRMT1 were added to a constant concentration of fluorescent peptide (0.2 μM) at 30°C in the same buffer mentioned above. The anisotropy increase due to the formation of large ES complexes was recorded with a Fluoro-Max 4 fluorimeter (Horiba Jobin Yvon). The excitation and emission wavelengths were set at 498 nm and 524 nm, respectively. Data were fit to eq 1, where $P$ is the fluorescence anisotropy at a given concentration of PRMT1, $A$ is the amplitude, and $k_d$ is the observed dissociation constant between PRMT1 ($E$) and H4 peptide ($S$).

$$P=A*\frac{(E+S+K_d)-\sqrt{(E+S+K_d)^2-4*E*S}}{2*S}+C \quad (1)$$

### Stopped-flow fluorescence measurements

The transient-state kinetics of association, dissociation and catalytic turnover were determined by stopped-flow fluorescence assays using several fluorescein-labeled H4 peptides (H4FL, H4FLme1, H4FLme2) as probes. Binding of the fluorescent peptide to PRMT1 (or PRMT1-cofactor complex) quenches the peptide fluorescence, while release of the peptide restores the fluorescence. The transient fluorescence signal change was detected at 30°C on an Applied Photophysics stopped-flow equipment using an excitation wavelength of 495 nm and a long pass emission filter centered at 510 nm. Four to six shots were collected and averaged for each curve. For the association measurements, increasing concentrations of PRMT1 (2, 4, 6 μM), with or without 100 μM SAH were mixed with 0.4 μM of fluorescent peptide in the reaction buffer (50 mM HEPES (pH 8.0), 50 mM NaCl, 1 mM EDTA, 0.5 mM DTT). After averaging the shot data, the association time courses were fitted to a single exponential function (eq 2) when the cofactor was absent, or to a double exponential function (eq 3) when the cofactor was present. In eq 2 and 3, $F$ is the fluorescence intensity at time $t$, $A$ is the amplitude of the fluorescence change, and $k_n$ are the rate constants. The observed rate constants were plotted against PRMT1 concentration, and the data were fit to eq 4 (in the absence of SAH) or eq 5 (in the presence of SAH) to derive the association rate constants $k_{on}$ or $k_1$, respectively. For eq 5, $k_1$ and $k_{-1}$ are the association and dissociation rate constants, and $k_2$ and $k_{-2}$ are the forward and reverse rate constants of phase 2.

$$F=A*\exp(-k*t)+C \quad (2)$$

$$F=A_1*\exp(-k_1*t)+A_2*\exp(-k_2*t)+C \quad (3)$$

$$k_{obs}=k_{on}*[\mathrm{PRMT1}]+k_{off} \quad (4)$$

$$k_{obs}=k_1*[\mathrm{PRMT1}]+k_{-1}+k_2+k_{-2} \quad (5)$$

For the dissociation rate constant measurements, 0.4 μM fluorescent peptide was prebound to 2 μM PRMT1 (with or without 100 μM SAH/SAM), and the complex was rapidly mixed

with 50 μM unlabeled H4(1–20) peptide to trap the free PRMT1. The averaged shot data were fitted to eq 2 when the cofactor is absent, or to eq 3 when the cofactor is present. Here $k$ (or $k_1$) is the dissociation rate constant ($k_{off}$), and $k_2$ reflects the rate constant for a putative conformational change before substrate release.

For PRMT1 methylation kinetics in single turnover conditions, H4FL or H4FLme1 peptides were used to probe the reaction rate for transfer of both methyl groups (H4FL) or only the second methyl group (H4FLme1). In these reactions, 2 μM PRMT1 and 100 μM SAM were mixed with 0.4 μM H4FL or H4FLme1 in the reaction buffer mentioned above. The methylation time course exhibited two distinct kinetic phases, and was fitted to a double exponential function (eq 3), where the observed $k_2$ likely reflects the methyl transfer rate constant. The rate constant for transfer of the first methyl group ($k_1'$) is calculated from eq 6, where $k_{tot}$ (the total rate constant for transfer of two methyl groups) is obtained from H4FL methylation time course, and $k_2'$ (the rate constant for transfer of the second methyl group) is obtained from H4FLme1 methylation time course.

$$1/k_{tot}=1/k_1'+1/k_2' \tag{6}$$

# RESULTS

## Oligomerization of PRMT1 stimulates its activity

To understand the process of methylation, we first checked the oligomeric state of PRMT1, as this enzyme has been reported to function as a homo-dimer or oligomers (33). Different concentrations of PRMT1 were incubated with glutaraldehyde (0.025%, v/v) for 5 min. 0.1% Triton X-100 was added to eliminate the nonspecific interactions. The mixtures were resolved using 8% SDS-PAGE and probed with anti-PRMT1 antibody. It is clear that as the protein concentration increases, the degree of oligomerization also increases until it reaches a plateau (Figure 1a, 1b). We further tested if there is a correlation between the activity of PRMT1 and its concentration. As Figures 1c and 1d reveal, the slope of a plot of the apparent $V_{max}$ divided by PRMT1 concentration (i.e. the apparent $k_{cat}$) is not constant as the PRMT1 concentration changes. In other words, the turnover rate per PRMT1 monomer becomes higher as its concentration increases, and then plateaus when it rises above ~0.5 μM. Together, these data suggest that PRMT1 oligomerization is dependent on concentration in the range of 0 to 0.5 μM, and that the final PRMT1 oligomeric complex is the most active form,

## H4 peptide synthesis and steady-state kinetic characterization

To create fluorescent probes for study of the PRMT-substrate interaction and methylation, we synthesized several peptides containing N-terminal 20 amino acids of histone H4, with 0, 1 or 2 methyl groups on Arg-3 and a fluorescein group on Dpr-10 (2,3-diaminopropionic acid residue, substituting for Leu-10) (Table 1). H4FL and H4FLme1 are substrates of PRMT1, and H4FLme2 is a product of PRMT1 catalysis. In this design, the fluorescein group is placed at an optimized position relative to the methylation site, such that the label does not affect substrate methylation but might still be sensitive to the local change in microenvironment induced by ligand binding. These fluorescent peptides were synthesized with the Fmoc-based solid phase peptide chemistry strategy, purified by HPLC, and analyzed by MALDI-MS.

After the peptide synthesis and characterization, we measured the steady-state kinetic parameters of PRMT1 catalysis with these substrates. [$^{14}$C]-SAM was used as the methyl donor for the methyltransferase reactions, enabling us to quantify the methylated products

by liquid scintillation counting. In the steady-state initial rate assays, one substrate concentration was varied and the other substrate was fixed in large excess (at least five-fold higher than its $K_m$) to ensure pseudo first-order reaction conditions. Each reaction was quenched at an appropriate time to ensure that substrate conversion was less than 20%. As shown in Table 2, the $K_m$ and $k_{cat}$ values of peptide for H4(1–20) and H4FL vary by less than three-fold, indicating that fluorophore does not significantly affect substrate methylation by PRMT1. Also, in a competitive fluorescence anisotropy assay, H4(1–20) was found to completely reverse the binding of H4FL to PRMT1 (Figure SI-1), indicating that the fluorescein-labeled peptide has the same binding mode to the enzyme as the label-free peptide. In addition, these synthesized peptide substrates exhibit comparable kinetic parameters as histone H4 protein, demonstrating that they are good representatives of H4 protein. The $k_{cat}/K_m$ values for un-methylated H4FL and mono-methylated H4FLme1 are $0.86 \pm 0.09\ \mu M^{-1}\ min^{-1}$ and $1.6 \pm 0.29\ \mu M^{-1}\ min^{-1}$, respectively, suggesting that PRMT1 has little preference for arginine-mono-methylated H4 peptide. The binding affinity between the fluorescein-labeled peptides and PRMT1 was measured by fluorescence anisotropy titrations (30), taking advantage of the fact that the large enzyme-peptide complex has a larger correlation time and higher anisotropy than the peptide ligand (Figure 2a and 2b). The $K_d$ values for the binding of H4FL, H4FLme1 and H4FLme2 to PRMT1 apoenzyme ($0.47 \pm 0.06\ \mu M$, $0.74 \pm 0.13\ \mu M$, and $0.44 \pm 0.09\ \mu M$, respectively) are very similar, suggesting that PRMT1 does not appreciably distinguish among the three peptide forms, although the $K_m$ of H4FLme1 ($0.17 \pm 0.03\ \mu M$) is somewhat lower than the other two peptides. It is possible that binding of cofactor SAM to PRMT1 alters its interaction with the peptide substrate.

## Measurement of the binding rate constants of the H4 peptides with PRMT1

Our fluorescein-labeled H4 peptide showed an appreciable fluorescence decrease when mixed with excess amounts of PRMT1, which was reversed by adding increasing concentrations of unlabeled H4(1–20) (Figure SI-2). This indicates a change in the environment for the fluorescein group upon substrate-enzyme interaction, and provides a signal to measure the association rate constant of the fluorescent peptide with PRMT1 using stopped flow fluorescence. In the transient kinetics experiments, the fluorescent peptide was rapidly mixed with increasing concentrations of PRMT1 (in large excess over the substrate), and the time-dependent fluorescence signal change was monitored to obtain the observed rate constants ($k_{obs}$). Typical time courses for H4FL, H4FLme1 and H4FLme2 are shown in Figures 3a, 3b, and 3c. Each averaged data curve was fitted well to a single-exponential function, suggesting no more than a simple single-step process. The $k_{obs}$ data were calculated and plotted against PRMT1 concentration (Figure 3d and Figure SI-3). The association rate constant ($k_{on}$) was obtained from the slope of the plot of $k_{obs}$ against PRMT1 concentration to be $40 \pm 1\ \mu M^{-1}s^{-1}$ for H4FL, $23 \pm 1\ \mu M^{-1}s^{-1}$ for H4FLme1, and $26 \pm 1\ \mu M^{-1}s^{-1}$ for H4FLme2.

## Measurement of dissociation rate constants of peptides from PRMT1

We next measured dissociation rate constants ($k_{off}$) of H4FL, H4FLme1, H4FLme2 from PRMT1. A trapping experiment was designed as previously described (34). In this measurement, one solution containing 0.4 μM fluorescent ligand and 2 μM PRMT1 was rapidly mixed with the other solution containing a large excess of unlabeled H4 peptide, *i.e.*, 50 μM of H4(1–20). Following mixing, the fluorescent ligand dissociated from the PRMT1 complex, and the free PRMT1 was trapped with excess H4(1–20). The single-exponential time course reflects this dissociation process, with the expected recovery of fluorescence of the labeled peptide as it is released to bulk solution (Figure 4). The dissociation rate constants obtained from these measurements are $333 \pm 9\ s^{-1}$ for H4FL, $292 \pm 3\ s^{-1}$ for H4FLme1, and $319 \pm 6\ s^{-1}$ for H4FLme2.

### Effect of SAH on enzyme binding and dissociation of H4FLme1

We also examined how the cofactor analog SAH affects the association and dissociation of the fluorescent substrate H4FLme1 with PRMT1. For the binding experiment, 100 μM of SAH was preincubated with PRMT1 (2, 4, and 6 μM) prior to rapid mixing with H4FLme1. The time course for PRMT1-SAH binding with H4FLme1 was monitored with stopped-flow fluorescence (Figure 5a). It is noted that the magnitude of the fluorescence change of H4FLme1 upon association with PRMT1-SAH is 2-fold larger than its binding with apo PRMT1 under the same condition (Figure 3b), and the association rate constant is two-fold higher (Table 3), indicating that SAH modulates the microenvironment of the fluorophore in the ES complex. More importantly, the time course data can only be fitted to a double exponential function, rather than a single exponential function as observed above, suggesting that the binding is not a single-step process and that minimally two steps are involved (Scheme 2b). The double exponential fitting produces two sets of $k_{obs}$, one for a fast phase and the other for a slow phase (phase 1 and phase 2 in Figure 5a, 5b). The rate constant values can be further fit to a two-step binding model (eq 5) (35). The first-step binding rate constant $k_1$ was determined from the slope of the fast phase as 48 ± 1 $\mu M^{-1}s^{-1}$. The plateau of the slow phase (36 ± 2 $s^{-1}$) corresponds to the sum of $k_2$ and $k_{-2}$, and the difference on the ordinate axis between this plateau and the intercept of the fast phase yields 117 ± 3 $s^{-1}$ for $k_{-1}$. Also, we measured the dissociation progression course for H4FLme1 from PRMT1 in the presence of 100 μM SAH (Figure 5c). Similar to the dissociation experiment for the H4FLme1—PRMT1 complex, excess H4(1–20) was used as the trapping ligand. Again, the dissociation time course could not be fitted to a single exponential function, confirming that the binding of H4FLme1 with PRMT1-SAH is not a single-step process. The two rate constants obtained from the double exponential fit (109 ± 1 $s^{-1}$ and 19 ± 0.2 $s^{-1}$) correspond to the two reverse rate constants in the two-step binding model ($k_{-1}$ and $k_{-2}$ in scheme 2b). Of note, the $k_{-1}$ value from the trapping experiment is very close to that obtained from the binding experiment, supporting the validity of the two-step model. Combining the kinetic data for binding and dissociation, all the four rate constants of scheme 2b were calculated. The $k_{off}$ for H4FLme1 dissociation from PRMT1-SAH complex is about three-fold lower than that of apo-PRMT1 (Table 3). In addition, the presence of 100 μM SAH or SAM was found to have a similar effect on the dissociation of H4FLme2 from the PRMT1-cofactor complex as described above (Figure 5d and Figure SI-4), lowering its $k_{off}$ to 204 ± 3 $s^{-1}$ or 163 ± 3 $s^{-1}$, respectively. The kinetic difference between H4 peptide binding to holo-PRMT1 and to apo-PRMT1 suggests that the presence of the cofactor modulates the PRMT1-substrate interaction.

### Progression of arginine methylation probed by stopped-flow fluorescence

Having determined the binding and dissociation rate constants of H4 substrates and products, we then investigated possible fluorescence signal changes that reflect PRMT1-mediated methylation. Toward this end, we measured the fluorescence changes of H4FL and H4FLme1 over the entire methylation reaction course (Figure 6a and 6b). In the stopped-flow experiments, a solution containing 2 μM PRMT1 and 100 μM SAM was mixed with a solution containing 0.4 μM fluorophore-labeled substrate to initiate the methylation. Such single-turnover conditions increase the chance of identifying active enzyme intermediates. Interestingly, a biphasic time course was observed. The fluorescence signal for the first phase decreased (phase I), and then gradually increased until a plateau was reached (phase II). A double exponential function was applied to determine the rate constants for the two phases (0.14 ± 0.01 $s^{-1}$ and 0.022 ± 0.001 $s^{-1}$ for the methylation of H4FL, and 7.2 ± 0.2 $s^{-1}$ and 0.034 ± 0.001 $s^{-1}$ for the methylation of H4FLme1). The second phase, *i.e.* the slower phase, likely reflects the methyl transfer step because the rate constants are in the same range as the $k_{cat}$ values measured from the steady-state experiments (0.43 ± 0.01 $min^{-1}$, 0.27 ± 0.01 $min^{-1}$, Table 2). Also, product release cannot contribute to the slow

phase given that the dissociation rate constants of H4FLme1 and H4FLme2 (Table 3) are several thousand-fold larger than the rate constants for the slow phase. On the other hand, the fast phase observed in the time course is of great interest. It does not relate to the substrate binding, because the observed first-order rate constants for binding of the substrate (*e.g.*, 248 ± 3 $s^{-1}$ for H4FLme1 at 2 μM of PRMT1 in presence of the cofactor) are significantly greater than the rate constants for phase I in the methylation experiments (*i.e.*, 0.14 ± 0.01 $s^{-1}$, 7.2 ± 0.2 $s^{-1}$). Indeed, if a closer look is taken at the very early part of the first phase (Figure 6a and 6b, inlets), an even faster phase can be discerned, which likely corresponds to the substrate binding step. Therefore, the first phase in the methylation course reveals a new step existing after the ternary complex formation, and prior to the methyl transfer step. Most likely, the newly discovered step corresponds to an enzyme isomerization step towards a catalytically active form in preparation for methyl transfer.

## DISCUSSION

The importance of PRMTs in biology and human disease is being increasingly recognized. In particular, PRMT1 is critically involved in cardiovascular disease and cancer, making it a potential therapeutic target for drug development. The mechanism of PRMT-catalyzed addition of methyl groups to histone and nonhistone substrates is central to our understanding of the action of arginine methylation in regulating chromatin function and signal transduction. Elucidation of the kinetic mechanism also facilitates better design of selective inhibitors of PRMTs.

Investigation of the transient kinetics of arginine methylation is limited by a lack of effective assay methods. The classic radioisotope-labeled assay for methyl transfer is not well suited for transient-state kinetic studies. Recently we found that fluorescein-labeled peptide substrates are sensitive to enzyme binding and the methylation reaction (30). Herein, we designed new fluorescein-labeled H4 peptides with different methylation states and carried out stopped flow fluorescence measurements to gain insights into substrate binding and arginine methylation. The steady-state kinetic parameters of these fluorophore-labeled substrates are close to that of the unlabeled H4 peptide and protein substrates, indicating that these peptides are ideal substrates to study PRMT catalysis. A high final PRMT1 concentration of 2 μM was used, where the enzyme is in its most active oligomeric state and which is a concentration high enough to prevent subunit dissociation upon dilution. It is also worth mentioning that we employed a non-limiting amount of SAM (100 μM) in the methylation reaction so that SAM binding was not rate limiting. Such a concentration is physiologically relevant because SAM concentration can be as high as 150–280 μM in the cell (36). Combining the stopped flow data for substrate and product association, dissociation, and for methylation, we proposed a minimal kinetic model as outlined in Scheme 3. A significant discovery from these transient kinetic measurements is the revelation of conformational transitions prior to and subsequent to the chemical step. The conformational change prior to the chemical step is reflected by the appearance of a fluorescence decay phase after substrate binding in the methylation time course, which is in turn faster than the subsequent methyl transfer step. The rate constant of this conformational phase in H4FL methylation progression course (0.14 ± 0.01 $s^{-1}$) is 3350-fold smaller than the observed H4FL—PRMT1 association rate constant (469 ± 10 $s^{-1}$ at 2 μM PRMT1), highlighting that the kinetic phase is not directly ascribed to substrate binding. This finding suggests that there is an unstable initial ES complex that is rapidly populated but has a low commitment to catalysis, and that the binding of substrate to PRMT1-SAM complex triggers a structural isomerization that likely transforms PRMT1 from a precatalytic state into a more active form poised for methyl transfer. Although structure analyses are needed to confirm the presence of a conformational change, the transient kinetics data clearly reveal a change in environment of the fluorophore in the ES complex that is suggestive of such an

isomerization. Therefore, the active site reorganization is requisite for initiation of the methyl transfer reaction. Thus far, detailed structural information on the PRMT1—H4 complex is absent, and consequentially, it is unknown how the substrate association alters the enzyme conformation. From the crystal structure of PRMT1, at least two loop motifs are present near the substrate binding site (33). We hypothesize that a conformational change occurs involving the movement of one or two flexible loops that exist predominantly in an open state in the precatalytic enzyme form (E form). Following the binding of substrate to the enzyme, the loop translocates and buries the active site to produce a closed, active enzyme form (E′ form) in preparation for the methyl transfer reaction.

The association/dissociation rate constants for H4FL, H4FL-me1 and H4FL-me2 are generally on the same scale (Table 3), indicating that PRMT1 has little discrimination among these peptides. Interestingly, the presence of SAH appreciably alters the kinetic mode and rate constants of substrate-PRMT1 binding and dissociation. For instance, the stopped-flow time course for association of H4FLme1 with the PRMT1-SAH complex, as well as the reverse dissociation process, do not follow single-exponential fitting, suggesting that the binding of H4FLme1 to PRMT1-SAH complex is not simply a single-step process. Instead, these transient kinetic data fit well to a double exponential function, yielding all four rate constants for the two phases. These results allow us to propose that H4FLme1 binds to the PRMT1-SAM or PRMT1-SAH complex in two steps: the first step involves rapid-equilibrium binding of the peptide ligand with the enzyme in an open state to form the initial ternary complex, and the subsequent step is a relatively slow change in enzyme conformation to form a closed-state of PRMT1. Notably, this conclusion coincides very well with the methylation kinetics study which also suggests a conformational step prior to the catalysis. It is conceivable that once the methyl transfer reaction is complete, the enzyme will return from the closed state to the open state through loop opening, allowing the release of the products (Scheme 3). At this stage, it is not clear how SAH or SAM structurally affects the interaction between PRMT and the peptide substrate. Based on the elevated $k_{on}$ and lowered $k_{off}$ in the presence of SAH or SAM (Table 3), the binding of SAH or SAM possibly modulates the conformation of PRMT1 such that more contact residues are exposed for substrate capture, which also makes the substrate bind to the enzyme more tightly. As observed in the crystal structure of CARM1, the apoprotein adopts an open state for SAM binding pocket, while the holoprotein in the SAH-bound state shows a closed conformation, as an essential H-bond is formed between Ser217 and Y154, (37, 38). Therefore, SAM and SAH are important regulators of PRMT-substrate interaction. An implication is that in order to identify unknown substrates of PRMTs in the cell, adding a sufficient amount of SAM/SAH would be beneficial.

The association and dissociation rate constants of H4 peptides are much faster than the chemical step in PRMT1 catalysis. This strongly supports the notion that transfer of the methyl group is the rate-limiting step along the reaction path. This result also confirms that PRMT1 likely follows a rapid equilibrium sequential mechanism for catalysis as previously proposed (28). Our data suggest that the monomethylated peptide H4FLme1 has a high chance to be released from PRMT1 before the second methyl group is added, because dissociation of H4FLme1 from either the apoenzyme ($292 \pm 3\ s^{-1}$) or the PRMT1-SAH complex ($109 \pm 1\ s^{-1}$) occurs much more frequently than its methylation ($0.034 \pm 0.001\ s^{-1}$). Thus PRMT1 likely transfers two methyl groups to the same arginine nitrogen in two independent processes. However, there may be more complex scenarios where this conclusion needs to be modified. For instance, a large monomethylated protein substrate could be partially bound to the enzyme through residues distal from the target arginine residue while still allowing the exchange of SAH with SAM for the second round of methyl transfer. Furthermore, in the cell, additional associated or accessory proteins in substrate complex or enzyme complex may augment enzyme-substrate interaction, thus connecting

the first and the second methylation reactions in one process. These scenarios warrant future investigation.

The rate constant for the transfer of the second methyl group ($0.034 \pm 0.001\ s^{-1}$) is about half that for the transfer of the first methyl group ($0.062 \pm 0.003\ s^{-1}$), suggesting that addition of the second methyl group to the same nitrogen of the arginine is more difficult than the first one, possibly because of steric hindrance for the nucleophilic attack. However, the rate for the conformational change following H4FLme1 binding ($7.2 \pm 0.2\ s^{-1}$) is faster than that of H4FL ($0.14 \pm 0.01\ s^{-1}$). Combining these two factors, catalysis of the second methyl group transfer has about the same turnover rate as that of the first methyl group. This correlates well with the steady-state kinetic data showing that H4FL and H4FL-me1 have similar $k_{cat}$ values ($0.43 \pm 0.01\ min^{-1}$ and $0.27 \pm 0.01\ min^{-1}$, respectively).

In this study we assumed that the set of H4FLme(0–2) probes mimic the kinetics of native H4 peptide and protein in PRMT1 catalysis since they showed similar steady-state kinetics (data in Table 2). However, we cannot rule out the possibility that the microsopic kinetic behavior of H4FLMe(0–2) probes may be slightly different from that of native H4 peptides, while still sharing similar steady-state kinetics behavior and having methylation as the rate-limiting step. Another interesting observation is that the $K_d$ values for H4FL, H4FL-me1 and H4FL-me2 are similar, yet the fluorescence anisotropy change of H4FLme1 binding to PRMT1 (0.053 ~ 0.109) is relatively larger than that for H4FL and H4FLme2 (0.053 ~ 0.087 and 0.053 ~0.080, respectively) (Figure 2). This is an interesting phenomenon that may reflect differences in the internal mobility of the bound fluorophores, or possibly that the active site structure of PRMT1 is subtly different in the H4FLme1-PRMT1 complex from that of H4FL- or H4FLme2-enzyme complex. This may also explain why the pre-catalytic conformational transition of H4FLme1 methylation reaction ($7.2 \pm 0.2\ s^{-1}$) is much faster than that of H4FL ($0.14 \pm 0.01\ s^{-1}$).

In conclusion, our stopped-flow fluorescence data provide a detailed view of arginine methylation catalyzed by PRMT1. Under this scheme, the methyl transfer step is the major rate-limiting step which proceeds much more slowly than substrate association/dissociation. Binding of cofactor SAM/SAH appreciably affects the interaction between H4 peptide and the enzyme, probably due to a conformational change upon enzyme-cofactor complex formation. Importantly, the transient kinetics data reveal a conformational transition step following the substrate binding and prior to the chemical step. This protein isomerization likely reorganizes the active site of PRMT1 from an open state to a closed state, activating the side-chain terminal nitrogen of H4R3 and/or the reactive methyl group of SAM to facilitate the methyl transfer. Further structural studies will be essential to validate this kinetic proposition.

## Supplementary Material

Refer to Web version on PubMed Central for supplementary material.

## Acknowledgments

This work was supported by NIH R01 grants GM086717 (YGZ) and GM068626 (JTS). MJ was supported by a Molecular Basis of Disease Fellowship at Georgia State University. MRS was supported by an Anticancer Drug Development Postdoctoral Fellowship from the National Cancer Institute.

## Abbreviations

**PTM** posttranslational modification

| | |
|---|---|
| **PRMT** | protein arginine methyltransferase |
| **SAM** | S-adenosyl-L-methionine |
| **MMA** | L-NMMA, ω-$N^G$ monomethylarginine |
| **ADMA** | ω-$N^G$,$N^G$-asymmetric dimethylarginines |
| **SDMA** | ω-$N^G$, $N'^G$-symmetric dimethylarginine |
| **SAH** | S-adenosyl-L-homocysteine |
| **RER** | rapid equilibrium random mechanism |
| **Dpr** | 2,3-diaminopropionic acid |
| **Fmoc** | N-(9-fluorenyl) methoxycarbonyl group |
| **SPPS** | solid phase peptide synthesis |
| **HCTU** | O-(1H-6-Chlorobenzotriazole-1-yl)-1,1,3,3-tetramethyluronium hexafluorophosphate |
| **DMF** | dimethylformamide |
| **TFA** | Trifluoroacetic acid |
| **HEPES** | 4-(2-hydroxyethyl)-1-piperazineethanesulfonic acid |
| **DTT** | dithiothreitol |
| **EDTA** | ethylenediaminetetraacetic acid |
| **PMSF** | phenylmethylsulfonyl fluoride |

## References


1. Pal S, Sif S. Interplay between chromatin remodelers and protein arginine methyltransferases. J Cell Physiol. 2007; 213:306–315. [PubMed: 17708529]
2. Lee DY, Teyssier C, Strahl BD, Stallcup MR. Role of protein methylation in regulation of transcription. Endocr Rev. 2005; 26:147–170. [PubMed: 15479858]
3. Krause CD, Yang ZH, Kim YS, Lee JH, Cook JR, Pestka S. Protein arginine methyltransferases: evolution and assessment of their pharmacological and therapeutic potential. Pharmacol Ther. 2007; 113:50–87. [PubMed: 17005254]
4. Gary JD, Clarke S. RNA and protein interactions modulated by protein arginine methylation. Prog Nucleic Acid Res Mol Biol. 1998; 61:65–131. [PubMed: 9752719]
5. Lee JH, Cook JR, Yang ZH, Mirochnitchenko O, Gunderson SI, Felix AM, Herth N, Hoffmann R, Pestka S. PRMT7, a new protein arginine methyltransferase that synthesizes symmetric dimethylarginine. J Biol Chem. 2005; 280:3656–3664. [PubMed: 15494416]
6. Zhang Y, Reinberg D. Transcription regulation by histone methylation: interplay between different covalent modifications of the core histone tails. Genes Dev. 2001; 15:2343–2360. [PubMed: 11562345]
7. Clarke S. Protein methylation. Curr Opin Cell Biol. 1993; 5:977–983. [PubMed: 8129951]
8. McBride AE, Silver PA. State of the arg: protein methylation at arginine comes of age. Cell. 2001; 106:5–8. [PubMed: 11461695]
9. Bauer UM, Daujat S, Nielsen SJ, Nightingale K, Kouzarides T. Methylation at arginine 17 of histone H3 is linked to gene activation. EMBO Rep. 2002; 3:39–44. [PubMed: 11751582]
10. Schurter BT, Koh SS, Chen D, Bunick GJ, Harp JM, Hanson BL, Henschen-Edman A, Mackay DR, Stallcup MR, Aswad DW. Methylation of histone H3 by coactivator-associated arginine methyltransferase 1. Biochemistry. 2001; 40:5747–5756. [PubMed: 11341840]

11. Wang H, Huang ZQ, Xia L, Feng Q, Erdjument-Bromage H, Strahl BD, Briggs SD, Allis CD, Wong J, Tempst P, Zhang Y. Methylation of histone H4 at arginine 3 facilitating transcriptional activation by nuclear hormone receptor. Science. 2001; 293:853–857. [PubMed: 11387442]
12. Pal S, Vishwanath SN, Erdjument-Bromage H, Tempst P, Sif S. Human SWI/SNF-associated PRMT5 methylates histone H3 arginine 8 and negatively regulates expression of ST7 and NM23 tumor suppressor genes. Mol Cell Biol. 2004; 24:9630–9645. [PubMed: 15485929]
13. Ma H, Baumann CT, Li H, Strahl BD, Rice R, Jelinek MA, Aswad DW, Allis CD, Hager GL, Stallcup MR. Hormone-dependent, CARM1-directed, arginine-specific methylation of histone H3 on a steroid-regulated promoter. Curr Biol. 2001; 11:1981–1985. [PubMed: 11747826]
14. Xu XHS, Mayo MW, Bekiranov S. Application of machine learning methods to histone methylation ChIP-Seq data reveals H4R3me2 globally represses gene expression. BMC Bioinformatics. 2010; 11:396. [PubMed: 20653935]
15. Chen D, Ma H, Hong H, Koh SS, Huang SM, Schurter BT, Aswad DW, Stallcup MR. Regulation of transcription by a protein methyltransferase. Science. 1999; 284:2174–2177. [PubMed: 10381882]
16. Fabbrizio E, El Messaoudi S, Polanowska J, Paul C, Cook JR, Lee JH, Negre V, Rousset M, Pestka S, Le Cam A, Sardet C. Negative regulation of transcription by the type II arginine methyltransferase PRMT5. EMBO Rep. 2002; 3:641–645. [PubMed: 12101096]
17. Yadav N, Lee J, Kim J, Shen J, Hu MC, Aldaz CM, Bedford MT. Specific protein methylation defects and gene expression perturbations in coactivator-associated arginine methyltransferase 1-deficient mice. Proc Natl Acad Sci U S A. 2003; 100:6464–6468. [PubMed: 12756295]
18. Zhu W, Mustelin T, David M. Arginine methylation of STAT1 regulates its dephosphorylation by T cell protein tyrosine phosphatase. J Biol Chem. 2002; 277:35787–35790. [PubMed: 12171910]
19. Bedford MT, Frankel A, Yaffe MB, Clarke S, Leder P, Richard S. Arginine methylation inhibits the binding of proline-rich ligands to Src homology 3, but not WW, domains. J Biol Chem. 2000; 275:16030–16036. [PubMed: 10748127]
20. Altschuler L, Wook JO, Gurari D, Chebath J, Revel M. Involvement of receptor-bound protein methyltransferase PRMT1 in antiviral and antiproliferative effects of type I interferons. J Interferon Cytokine Res. 1999; 19:189–195. [PubMed: 10090404]
21. Tang J, Kao PN, Herschman HR. Protein-arginine methyltransferase I, the predominant protein-arginine methyltransferase in cells, interacts with and is regulated by interleukin enhancer-binding factor 3. J Biol Chem. 2000; 275:19866–19876. [PubMed: 10749851]
22. McBride AE, Weiss VH, Kim HK, Hogle JM, Silver PA. Analysis of the yeast arginine methyltransferase Hmt1p/Rmt1p and its in vivo function. Cofactor binding and substrate interactions. J Biol Chem. 2000; 275:3128–3136. [PubMed: 10652296]
23. Meister G, Eggert C, Buhler D, Brahms H, Kambach C, Fischer U. Methylation of Sm proteins by a complex containing PRMT5 and the putative U snRNP assembly factor pICln. Curr Biol. 2001; 11:1990–1994. [PubMed: 11747828]
24. Friesen WJ, Paushkin S, Wyce A, Massenet S, Pesiridis GS, Van Duyne G, Rappsilber J, Mann M, Dreyfuss G. The methylosome, a 20S complex containing JBP1 and pICln, produces dimethylarginine-modified Sm proteins. Mol Cell Biol. 2001; 21:8289–8300. [PubMed: 11713266]
25. Wysocka J, Allis CD, Coonrod S. Histone arginine methylation and its dynamic regulation. Front Biosci. 2006; 11:344–355. [PubMed: 16146736]
26. Torres-Padilla ME, Parfitt DE, Kouzarides T, Zernicka-Goetz M. Histone arginine methylation regulates pluripotency in the early mouse embryo. Nature. 2007; 445:214–218. [PubMed: 17215844]
27. Ancelin K, Lange UC, Hajkova P, Schneider R, Bannister AJ, Kouzarides T, Surani MA. Blimp1 associates with Prmt5 and directs histone arginine methylation in mouse germ cells. Nat Cell Biol. 2006; 8:623–630. [PubMed: 16699504]
28. Obianyo O, Osborne TC, Thompson PR. Kinetic mechanism of protein arginine methyltransferase 1. Biochemistry. 2008; 47:10420–10427. [PubMed: 18771293]
29. Lakowski TM, Frankel A. A kinetic study of human protein arginine N-methyltransferase 6 reveals a distributive mechanism. J Biol Chem. 2008; 283:10015–10025. [PubMed: 18263580]

30. Feng YXN, Wu J, Yang C, Zheng YG. Inhibitory study of protein arginine methyltransferase 1 using a fluorescent approach. Biochem Biophys Res Commun. 2009; 379:567–572. [PubMed: 19121292]

31. Xie N, Elangwe EN, Asher S, Zheng YG. A dual-mode fluorescence strategy for screening HAT modulators. Bioconjug Chem. 2009; 20:360–366. [PubMed: 19146394]

32. Feng Y, Li M, Wang B, Zheng YG. Discovery and mechanistic study of a class of protein arginine methylation inhibitors. J Med Chem. 2010; 53:6028–6039. [PubMed: 20666457]

33. Zhang XCX. Structure of the predominant protein arginine methyltransferase PRMT1 and analysis of its binding to substrate peptides. Structure. 2003; 11:509–520. [PubMed: 12737817]

34. Zheng YMF, Toptygin D, Brand L, Stivers JT, Cole PA. Fluorescence analysis of a dynamic loop in the PCAF/GCN5 histone acetyltransferase. Biochemistry. 2005; 44:10501–10509. [PubMed: 16060659]

35. Johnson KA. Transient-State Kinetic Analysis of Enzyme Reaction Pathways. The Enzymes. 1992; 20:1–61.

36. Balaghi M, Horne DW, Wagner C. Hepatic one-carbon metabolism in early folate deficiency in rats. Biochem J. 1993; 291(Pt 1):145–149. [PubMed: 8471033]

37. Yue WWHM, Roe SM, Thompson-Vale V, Pearl LH. Insights into histone code syntax from structural and biochemical studies of CARM1 methyltransferase. EMBO J. 2007; 26:4402–4412. [PubMed: 17882261]

38. Troffer-Charlier NCV, Hassenboehler P, Moras D, Cavarelli J. Functional insights from structures of coactivator-associated arginine methyltransferase 1 domains. EMBO J. 2007; 26:4391–4401. [PubMed: 17882262]

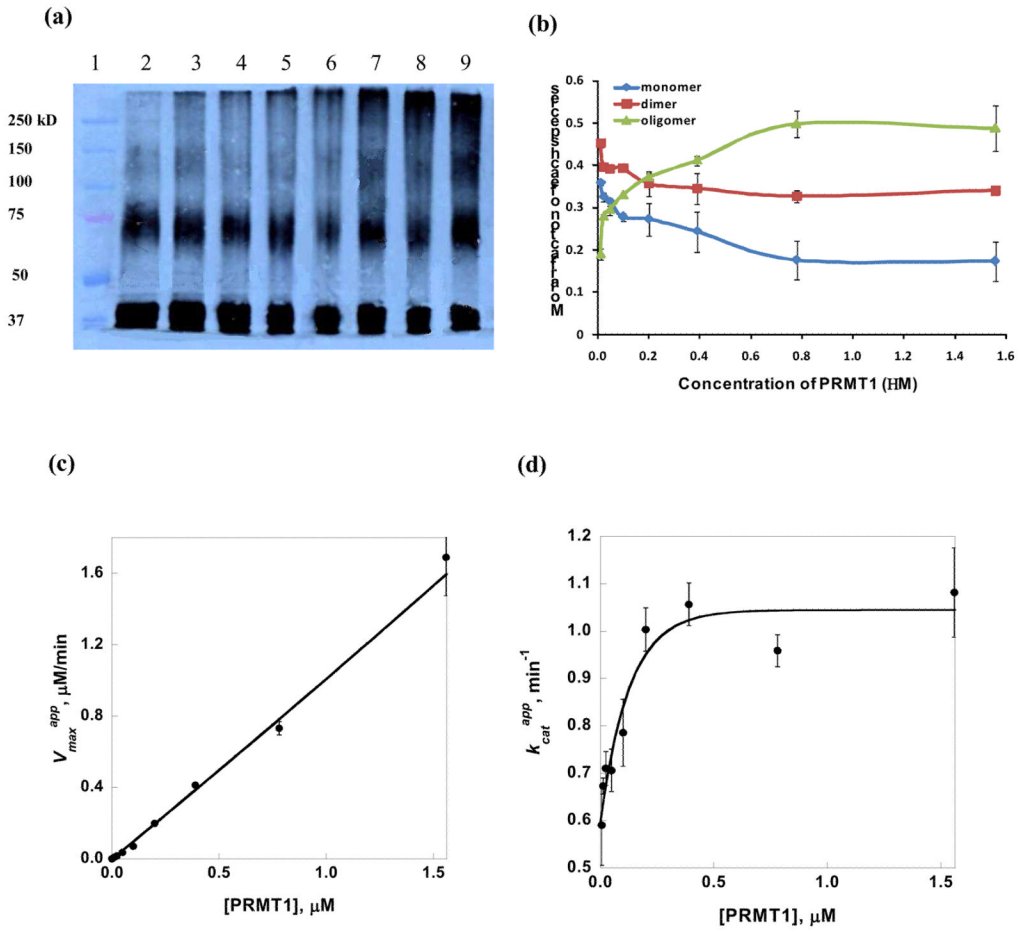


**Figure 1.**

Concentration dependence of PRMT1 oligomerization and catalytic activity. (a) Western blot analysis of PRMT1 oligomerization. Different concentrations of PRMT1 (0.012 μM — 3.13 μM) were prepared in presence of 0.1% Triton X-100 and incubated with 0.025% (v/v) glutaraldehyde for 5 min. The crosslinked proteins were resolved on 8% SDS-PAGE followed by western blot detection (primary antibody: anti-PRMT1 rabbit polyclonal IgG; secondary antibody: goat anti-rabbit IgG-HRP). Lane 1 to 9: marker, 0.012 μM, 0.024 μM, 0.05 μM, 0.10 μM, 0.20 μM, 0.39 μM, 0.78 μM, and 1.56 μM of PRMT1. (b) Concentration-dependent oligomerization of PRMT1. The western blot densitometry was analyzed by *QuantityOne* software, and the fractions of PRMT1 monomer, dimer and oligomer were plotted as a function of PRMT1 concentration. (c) Maximum velocity as a function of PRMT1 concentration. 0 ~ 3.13 μM of PRMT1 was added to the reaction buffer containing 18.75 μM of [$^{14}$C]-SAM and 18.75 μM of H4–20. The total protein concentration for each reaction was controlled at 3.13 μM by including BSA as a carrier protein, eliminating the effect of nonspecific interaction. Each reaction was quenched at less than 20% yield. (d) Apparent $k_{cat}$ as a function of PRMT1 concentration. The data were deduced from (c) by dividing the maximum velocity with the corresponding enzyme concentration.

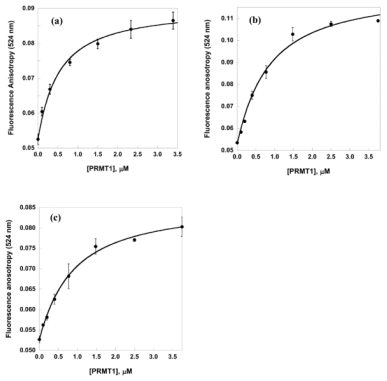


**Figure 2.**

Fluorescence anisotropy titration of fluorescent peptides with PRMT1. 0.2 μM of H4FL (a), H4FLme1 (b) or H4FLme2 (c) was titrated with increasing concentration of PRMT1 at 30°C in the reaction buffer mentioned above, and the anisotropy change due to large ES complex formation was recorded, with 498 nm excitation and 524 nm emission. Data were fit to eq 1 to calculate the $K_d$ values.

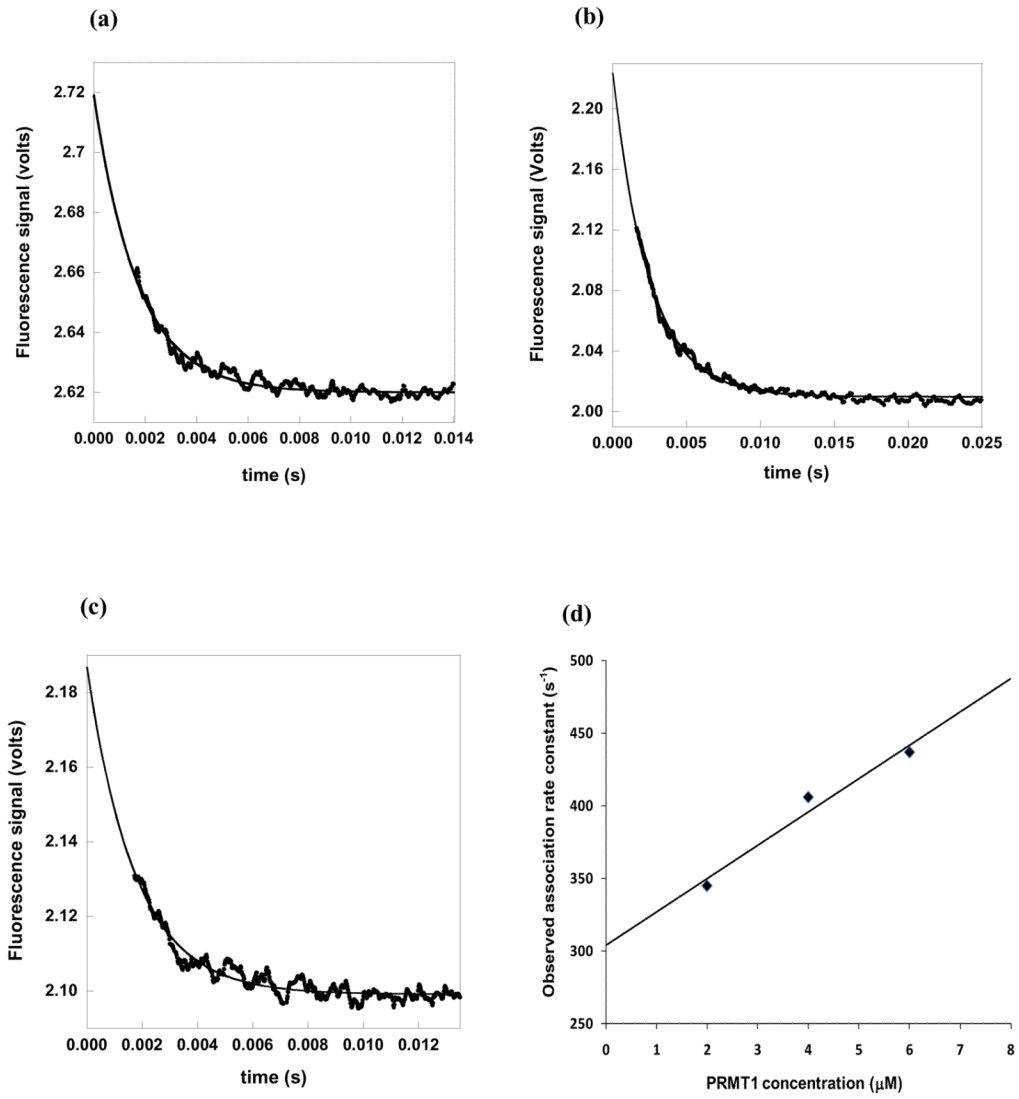


**Figure 3.**

Stopped-flow measurements of peptide association with PRMT1. Panel (a), (b), and (c) show the fluorescence change of H4FL, H4FLme1, and H4FLme2 (0.4 μM) upon mixing with PRMT1 (4 μM) at 30 °C in the reaction buffer, respectively. Excitation wavelength was selected at 495 nm and emission ≥510 nm was detected. Each sample was injected 4 to 6 times. The black dots show the averaged data points, and the curves are fit with eq 2. Panel (d) shows the observed association rate constant of H4FLme1 plotted against the concentration of PRMT1. The data were fit to linear eq 4.

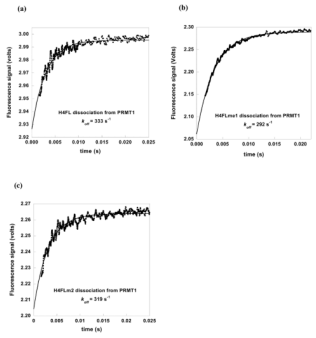


**Figure 4.**

Stopped-flow measurements of peptide dissociation from PRMT1. 0.4 μM fluorescent peptide was premixed with 2 μM PRMT1 in the reaction buffer. The solution was then rapidly mixed with 50 μM H4(1–20) on stopped-flow instrument at 30 °C. Each sample was injected 4 to 6 times. The black dots show the averaged data points, and the curves are fit with eq 2. (a), (b), and (c) show the dissociation time course of H4FL, H4FLme1, and H4FLme2 from PRMT1, respectively.

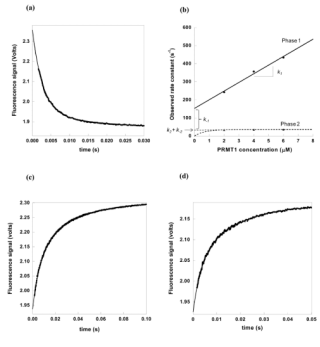


**Figure 5.**

Effect of SAH on the binding and dissociation of H4 substrate. Panel (a) shows the fluorescence change of H4FLme1 (0.4 μM) upon mixing with a solution containing 4 μM PRMT1 and 100 μM SAH at 30 °C in the reaction buffer. The data are fit with a double-exponential function (eq 3). The observed rate constants for phase 1 and phase 2 are plotted against the concentration of PRMT1 (or PRMT1-SAH complex), and the data are fit to eq 5 to get the four rate constants for the two phases, as shown in panel (b). Panel (c) and (d) show the dissociation time course of H4FLme1 and H4FLme2 from PRMT1-SAH complex, respectively. 0.4 μM fluorescent peptide was premixed with 2 μM PRMT1 and 100 μM SAH in the reaction buffer. The solution was then rapidly mixed with 50 μM H4(1–20) on stopped-flow instrument. The data are fit to eq 3.

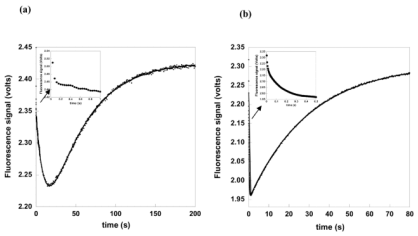


**Figure 6.**

Time course of PRMT1 catalysis probed by stopped-flow fluorescence. (a) H4FL was used to probe the progression of two methyl transfer; and (b) H4FLme1 was used to detect the progression of the second methyl transfer. In both measurements, 0.4 μM fluorescent peptide was mixed with a solution containing 2 μM PRMT1 and 100 μM SAM at 30°C in the reaction buffer. Each reaction was performed 4 to 6 times, and the black dots show the averaged data points. The data are fit with eq 3. Inset graphs magnify the data points at the very early stage of the reaction.

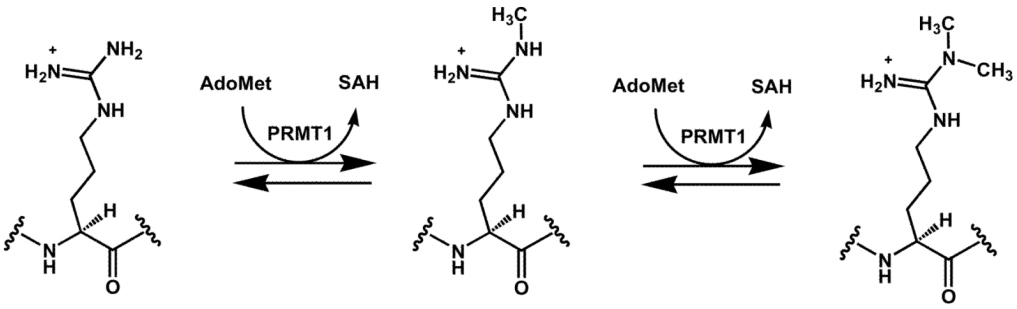


**Scheme 1.**
PRMT1-catalyzed arginine methylation.

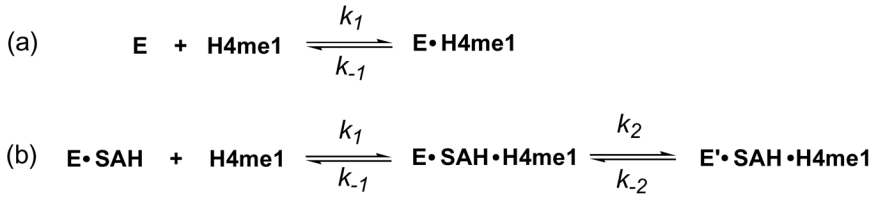


**Scheme 2.**

Two different kinetic models of substrate association with PRMT1 apoenzyme and holoenzyme. **(a)** single-step binding model between H4FLme1 and PRMT1. (b) two-step binding model between H4FLme1 and PRMT1-SAH complex. E: open-state PRMT1. E′: closed-state PRMT1.

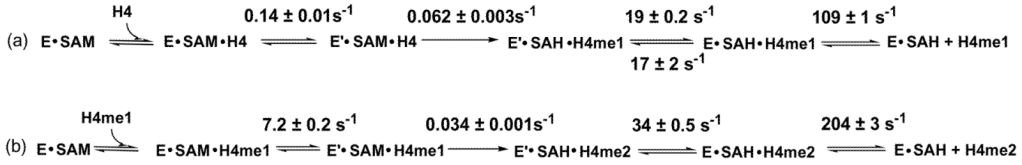


**Scheme 3.**

Proposed minimal kinetic model of PRMT1 catalysis. (a) first methylation and (b) second methylation of H4. The chemical step is rate-limiting. E: open-state PRMT1. E′: closed-state PRMT1.

**Table 1**

Sequences of H4 peptides. Dpr: 2,3-diaminopropionic acid residue; FL: fluorescein group; me: methyl group.

| Peptide name | Sequence |
|---|---|
| H4(1–20) | Ac-SG**R**GKGGKGLGKGGAKRHRK |
| H4FL | Ac-SG**R**GKGGKGDpr(FL)GKGGAKRHRK |
| H4FLme1 | Ac-SG$\mathbf{R}_{me1}$GKGGKGDpr(FL)GKGGAKRHRK |
| H4FLme2 | Ac-SG$\mathbf{R}_{me2}$GKGGKGDpr(FL)GKGGAKRHRK |

## Table 2

Steady-state kinetic characterization of PRMT1 binding and catalysis. The radioactive methylation assays were carried out at 30°C and pH 8.0. PRMT1 Concentration was typically 0.01 μM in the catalytic experiments. $K_d$ values were detected in fluorescence anisotropy titration using constant fluorescent peptide (0.2 μM) and increasing concentration of PRMT1.

| Substrates | $K_m$, μM | $k_{cat}$, $min^{-1}$ | $k_{cat}/K_m$, $\mu M^{-1}$ $min^{-1}$ | $K_d$, μM |
|---|---|---|---|---|
| H4 protein | 1.69 ± 0.39 | 0.50 ± 0.03 | 0.30 ± 0.07 | - |
| H4(1–20) | 0.64 ± 0.04 | 0.81 ± 0.01 | 1.27 ± 0.08 | - |
| H4FL | 0.50 ± 0.05 | 0.43 ± 0.01 | 0.86 ± 0.09 | 0.47 ± 0.06 |
| H4FLme1 | 0.17 ± 0.03 | 0.27 ± 0.01 | 1.60 ± 0.29 | 0.74 ± 0.13 |
| H4FLme2 | - | - | - | 0.44 ± 0.09 |
| SAM (for H4FL methylation) | 3.10 ± 0.46 | 0.48 ± 0.02 | 0.15 ± 0.02 | - |
| SAM (for H4FLme1 methylation) | 1.59 ± 0.37 | 0.33 ± 0.02 | 0.21 ± 0.05 | - |

**Table 3**

Summary of rate constant data obtained from stopped-flow fluorescence measurements.

| Rate constants / Peptides | Association with PRMT1 | Association with PRMT1-SAH | Dissociation from PRMT1 | Dissociation from PRMT1-SAH | Dissociation from PRMT1-SAM | First phase in the course of methylation | Second phase in the course of methylation |
|---|---|---|---|---|---|---|---|
| H4FL | 40 ± 1 $\mu M^{-1}s^{-1}$ | - | 333 ± 9 $s^{-1}$ | - | - | 0.14 ± 0.01$s^{-1}$ | 0.022 ± 0.001 $s^{-1}$ |
| H4FLme1 | 23 ± 1 $\mu M^{-1}s^{-1}$ | 48 ± 1 $\mu M^{-1}s^{-1}$* | 292 ± 3 $s^{-1}$ | 109 ± 1 $s^{-1}$* | - | 7.2 ± 0.2 $s^{-1}$ | 0.034 ± 0.001 $s^{-1}$ |
| H4FLme2 | 26 ± 1 $\mu M^{-1}s^{-1}$ | - | 319 ± 6 $s^{-1}$ | 204 ± 3 $s^{-1}$* | 163 ± 3 $s^{-1}$* | - | - |

*indicates the rate constant for the fast phase (phase 1) calculated from double-exponential fitting.